Journal of Materials Science: Materials in Electronics (2018) 29:15946–15956
https://doi.org/10.1007/s10854-018-9680-1

Graphene oxide based free-standing films for humidity and hydrogen peroxide sensing

Pranay Ranjan[1] · Punam Tiwary[2,3] · Amit K. Chakraborty[3] · R. Mahapatra[2] · Ajay D. Thakur[1]

Received: 4 June 2018 / Accepted: 16 July 2018 / Published online: 20 July 2018

Abstract
We have synthesized free-standing films of graphene oxide (GO), reduced graphene oxide (rGO) and graphene oxide-manganese oxide composite (GMC) for humidity and hydrogen peroxide sensing applications. Structural and morphological characterizations of these free-standing films were performed using X-ray diffraction (XRD), Raman spectroscopy and scanning electron microscopy (SEM). The presence of anionic sites in the form of oxygen functional groups (OFGs) at the surface of GO along with its hydrophilic nature makes GO a unique candidate as a suitable material for humidity and hydrogen peroxide sensing. In contrast, rGO has a relatively lower fraction of OFGs, higher electrical conductivity and hydrophobicity compared to GO. We estimate the response time, recovery time and stability of free-standing films over multiple sensing-degassing cycles of the as chemically prepared GO, rGO and GMC films for humidity sensing. We observed a dramatic improvement in both the response and recovery times for rGO and GMC films compared to GO film at relatively low humidity, while at higher humidity percentages, rGO film has the best response and recovery times compared to GMC and GO films. Regarding stability, GO was found to be more stable over multiple sensing cycles compared to rGO and GMC at high humidity values. In addition to this, we observed that the addition of metal oxide to GO makes GMC film more selective for hydrogen peroxide sensing in comparison to GO and rGO film at a lower concentration.

1 Introduction

Detection of humidity (H_2O) and hydrogen peroxide (H_2O_2) concentrations is highly desirable for food packaging industry, environmental monitoring, and medicine/medical science [1, 2]. Use of H_2O monitoring is not only limited to the packaging industry, environmental monitoring, and medicine/medical science, it is also used in general day to day life, e.g., in a microwave oven for cooking control, for respiratory equipment, greenhouse air conditioning, soil moisture monitoring, gas purification and incubators [3–5]. On the other hand, H_2O_2 is used extensively in food preservation and packaging industries as an antimicrobial agent (including perishable food items which constitute a familiar daily source of nutrition like milk) [6] and as a sterilizing agent in most packaged food items [3]. It is also used as a bleaching agent in wheat flour, egg white, and edible oil (due to its strong oxidizing property). Ingestion of 3% concentration of H_2O_2 can lead to vomiting, burns in throat, mouth or irritation to the mucosa while consumption of higher concentrations (above 10%) can lead to severe burns to mucous membranes [7, 8]. In its anhydrous form, H_2O_2 is easy to detect because of its bitter taste and pungent odor. However, it is difficult to sense its presence in aqueous form at lower concentrations. What makes it more difficult to trace is that if it comes in contact with food, it quickly gets decomposed. Till date, various methods of sensing like resistive, capacitive, acoustic, mechanical and optical based techniques have been implemented for sensing of H_2O while for sensing of H_2O_2, the techniques include electrochemical sensing [9–12], photometry [13], chemiluminescence [14],

✉ Pranay Ranjan
pranjan@iitp.ac.in

✉ Amit K. Chakraborty
amit.chakraborty@phy.nitdgp.ac.in

✉ Ajay D. Thakur
ajay.thakur@iitp.ac.in

[1] Department of Physics, Indian Institute of Technology Patna, Bihta 801106, India

[2] Department of Electronics and Communication Engineering, National Institute of Technology, Durgapur, Durgapur 713209, India

[3] Carbon Nanotechnology Lab, Department of Physics, National Institute of Technology, Durgapur, Durgapur 713209, India

and spectrometry [15]. Even though each of the sensing methods possesses some unique properties, the integration of these systems in real-time is not cost effective. Expensive lithography technique and use of expensive experimental tools for detection of the analyte are central obstructions to overcome. Moreover, robustness, sensitivity and operating temperature are some of the other parameters which need to be optimized. Amongst all the techniques mentioned above, resistive sensors rely on the principle of sensing through a sharp change in its resistance upon adsorption of an analyte gas. It is thus a simple and effective technique to detect an analyte. It, therefore, received much attention due to its simplicity and cost-effectiveness as well as the choice of various sensing materials and hence is also the focus of the present study.

Use of nanostructured materials opens a new domain for sensing due to their high surface to volume ratio, surface reactivity, and ability to tune and functionalize the surface charge for getting an improved response to a particular analyte. Literature suggests materials for sensing includes ceramics, polymers, hybrids, composites, organic compounds [16, 17], etc. Due to high operating temperature, use of ceramics (metal oxides) is limited for humidity sensing, while polymers or organic compound based sensors lack in stability. In recent years, graphene has emerged as a good sensing material [18–23] due to its high conductivity, charge mobility, mechanical and chemical stability [24, 25]. However, lack of functional groups and defects limit the sensing response of intrinsic graphene despite the above mentioned exciting properties. Graphene oxide (GO) which contains ample functional groups thus provides an alternative for increasing the sensitivity and selectivity of graphene to various analyte species [26] also modified electrode with nanostructured materials including graphene, graphene oxide, and reduced graphene oxide has been widely explored [6, 27–39].

Graphene or GO functionalized with metal oxide nanoparticles have been widely reported to reduce the operating temperature of the sensor as well as to improve the overall sensitivity due to the synergetic advantages of metal oxides and graphene [40]. However, most of these reports use functionalized graphene or GO-based films supported on some substrates [41]. For example, in recent work by Naik and Krishnaswamy [42] demonstrated a GO-based resistive humidity sensor that works at room temperature whereas, Borini et al. [43] reported an ultrafast humidity sensor based on thin GO film.

Similarly, H_2O_2 has been detected previously by electrochemical methods using various metals and metals hybrids [44]. Parts per million sensitive chemiresistive sensors to detect vapor of H_2O_2 has also been reported [44], but there is no report on liquid H_2O_2 detection by the chemiresistive sensor of GO.

According to our literature review, there are no reports on humidity and hydrogen peroxide sensors using free-standing GO films. Also, the free-standing film offers excellent flexibility as chemiresistive sensors, therefore in this work we have synthesized free-standing GO films for sensing of humidity and hydrogen peroxide. GMC films are made using a composite of GO with MnO_2 and are investigated further for sensing of H_2O and H_2O_2.

2 Experimental details

2.1 Materials

Graphite (C) and potassium permanganate ($KMnO_4$) were procured from CDH laboratory chemicals (India). Orthophosphoric acid (H_3PO_4), sulphuric acid (H_2SO_4) and hydrogen peroxide (H_2O_2) were purchased from Sigma-Aldrich whereas manganese oxide (MnO_2) was procured from Alfa Aesar. All the chemicals were used without any further treatment or purification. All the solutions were prepared using double de-ionized (DI) water and its ice.

2.2 Synthesis of the sensor material

GO film was prepared using improved Hummer's method [45–48]. It involved three crucial steps: intercalation, oxidation, and exfoliation [45–47]. Graphite (C) and $KMnO_4$ was made in the ratio of 1:6 and were crushed in a mortar and pestle. In a separate beaker, a mixture of H_2SO_4 and H_3PO_4 was made in 9:1 ratio which was added to the C and $KMnO_4$ mixture under continuous stirring and heated for 24 h at 65 °C. Suitable precautions were taken to avoid any explosion [47, 48]. The reaction was terminated using H_2O_2 and DI water (ice) after 24 h. In this process, intercalation was started as soon as $KMnO_4$ was crushed with C, while oxidation started after addition of acids. H_2O_2 was added for termination of the reaction, and completion of exfoliation since it is a potent oxidizing agent. The obtained sample was washed in succession with water, ethanol and hydrochloric acid [47]. The resultant material after washing was found to be in the form of a slurry which was then degassed very slowly in a petri-dish using a rotary pump to evaporate the solvent and get the free-standing films of GO (Fig. 1). The same free-standing film was reduced by irradiating under UV lamp (12 W) for 32 h to get rGO free-standing film. Further, we mixed 15 wt% of MnO_2 with GO in ethanol and stirred for 2 h followed by degassing in the same manner as for GO to obtain a free-standing film of graphene manganese oxide composite (GMC) film. Photographs of the free-standing films of GO, rGO, and GMC are depicted in Fig. 1 which reveals a good mixture of MnO_2 particles over the surface of the GMC film.

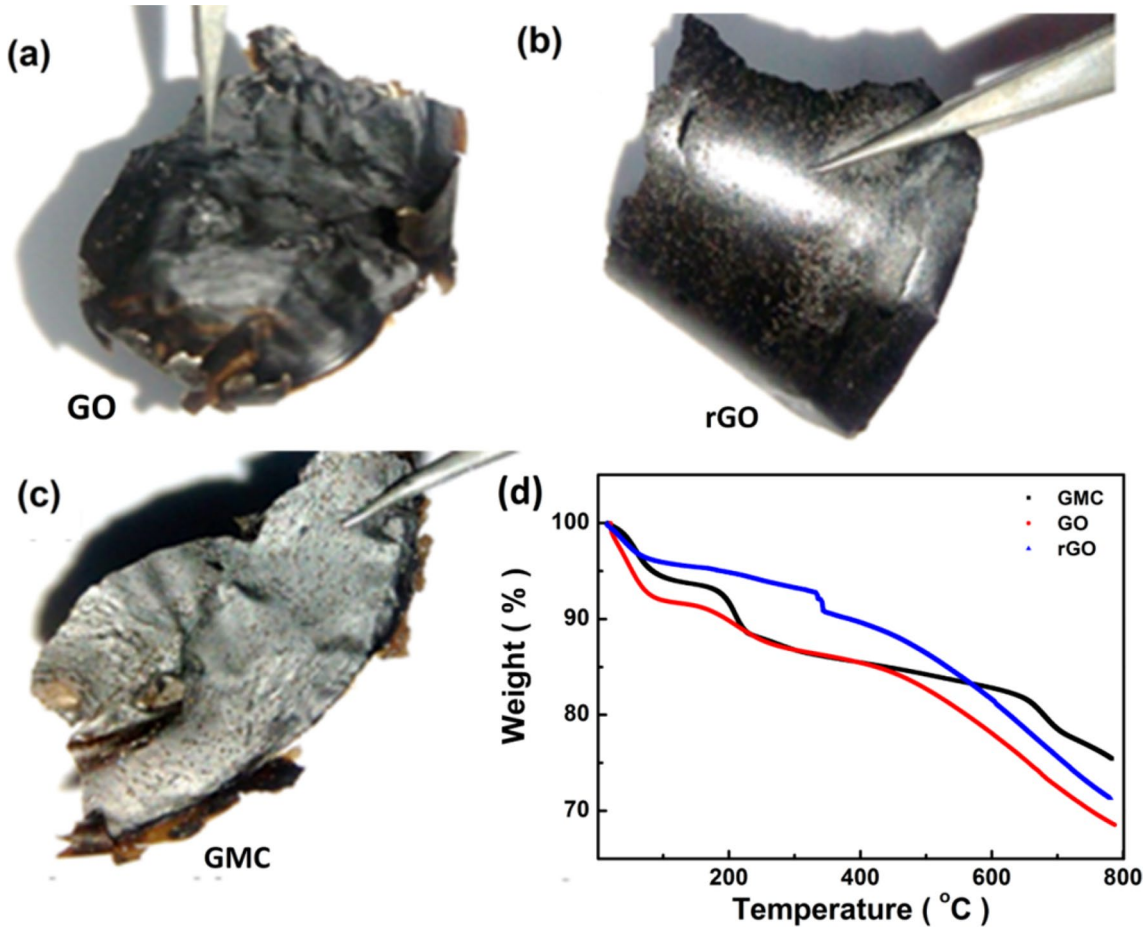

Fig. 1 Digital photographs of free-standing films of **a** GO, **b** rGO, **c** GMC respectively and **d** TGA profile of GO, rGO, and GMC

Figure 1d shows the TGA profile of GO, rGO, and GMC powder. TGA was performed to know about the thermal stability of the sample. We observed that GO has lower thermal stability in comparison to rGO and GMC [49–51]. GO starts to lose mass at 90 °C, which is the attributed to the adsorb relative humidity from the ambiance, while a significant change in mass is observed at 165 °C (due to loss of oxygen functional groups). On contrary rGO and GMC film showed higher thermal stability of 5 and 8% weight loss at 328 and 187 °C respectively. Overall, GMC film has higher thermal stability as compared to GO and rGO due to the presence of metal oxides, which are relatively more stable as compared to GO and rGO.

A free-standing film do not require any substrate for the fabrication of gas sensor. We used GO, rGO and GMC films directly as a device and connected it to the clip for making an electrode thus, making the system simple to use and reducing the overall cost of the sensor.

2.3 Sensing measurement

2.3.1 Humidity sensing

The fabricated devices were enclosed in a customized gas sensor platform (Bat-Sol Pvt. Ltd.) containing a sample chamber (6.7 L volume) made of steel to accommodate the sensor as shown in Fig. 2a. Figure 2b represents a gas sensor chamber set up for hydrogen peroxide analyte sensing. In the humidity sensing measurement dry air was used to check the baseline response with the help of nitrogen and oxygen. We monitored the amount of humidity with the help of a digital hygrometer (HTC Thermo Hygrometer). All humidity sensing measurements were made at room temperature (27 °C). The sensor film was placed inside the stainless steel container and was connected with two probes whose other ends were connected to a multimeter through a vacuum sealed feed through. Change in resistance across the two electrodes was monitored by a digital multimeter (Chroma

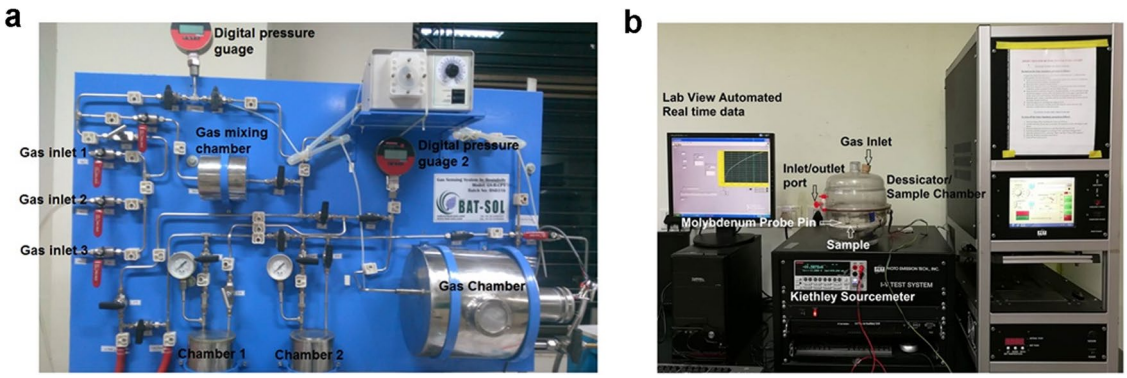

Fig. 2 Photographs showing the gas sensing instruments for **a** humidity and **b** H_2O_2

12061) interfaced with a computer with the help of a USB test and measurement cable.

The chamber was first degassed at 10^{-5} torr (for this vacuum was created using a diffusion pump backed with a rotary vane pump), followed by localized heating (30 min) so that no humidity content is present in the chamber. After flushing with nitrogen gas, the sample was inserted inside the chamber, followed by evacuation to a pressure of 10^{-5} torr. Nitrogen and oxygen gas mixture (7:3 v:v) was then flown into the chamber to 1 atm. pressure. The resistance of the film did not change upon introduction of this gas mixture and hence was used as the reference for sensing measurement. The ambient humid air was inserted into the chamber directly from the atmosphere. The response of the film was calculated by using the equation,

$$\text{Response} = R_a/R_g \tag{1}$$

where R_a and R_g are the resistances of the film before and after the exposure of humidity, respectively.

2.3.2 Hydrogen peroxide sensing

All electrical measurement related to hydrogen peroxide sensing was performed at room temperature in 10^{-3} torr pressure using Keithley 2420 sourcemeter. The pressure inside the chamber was achieved with the help of a rotary pump. Analyte source was taken in aqueous form and injected with the help of a syringe in a closed chamber. Gas concentration in ppm corresponding to the amount of liquid was estimated using Eq. (2) [18].

$$c = \frac{22.4\rho TV_s}{273MV} \times 1000 \tag{2}$$

where, C is the concentration of gaseous hydrogen peroxide (ppm), T is the testing temperature or operating temperature in Kelvin, ρ is the density of liquid hydrogen peroxide (g mL^{-1}), V_s is the volume of liquid hydrogen peroxide (μL), M is the molecular weight of hydrogen peroxide (g mol^{-1}) and V is the volume of the chamber (L). To minimize the problem of cross-sensitivity due to the presence of metals in contact pads or wires, we covered all the contact pads and wires by adhesives and then measured the response of our free-standing film in the vacuum. The idea is to get a response only from the sensing film by minimizing the effect of metal contact pads.

2.4 Characterization of the free-standing film

The obtained free-standing film or paper films of GO, rGO,and GO-MnO_2 (GMC) were characterized by X-ray diffraction (Rigaku TTRAX III) with CuKα (1.54 Å) radiation. Raman spectra were recorded for all samples in the wave number range of 150–3100 cm^{-1} in back scattering geometry using a confocal Micro-Raman spectrometer (Seki Technotron, Japan) powered by an Argon ion laser source emitting 514 nm radiation. Structural and morphological analyses of the samples were performed using a Carl-Zeiss Sigma scanning electron microscope (SEM).

3 Results and discussion

3.1 XRD, Raman and SEM characterization

Figure 3a shows the XRD pattern of GO free-standing film (bottom panel). The peak observed at $2\theta = 9.11$ Å corresponds to 002 planes of GO [46–48]. Centre panel of Fig. 3a represents the XRD pattern of rGO free-standing film in which abroad hump can be observed at $2\theta = 25.1°$ [52, 53] which indicates the successful reduction of GO [47].Similarly, the top panel of Fig. 3a shows the XRD pattern of the GMC free-standing film in which a weak peak due to MnO_2 is observed at $2\theta = 48.88°$ in addition to the one at 9.78° due to GO.

Figure 3b shows the observed Raman spectra of GO, rGO and GMC free-standing film in the wavenumber range of

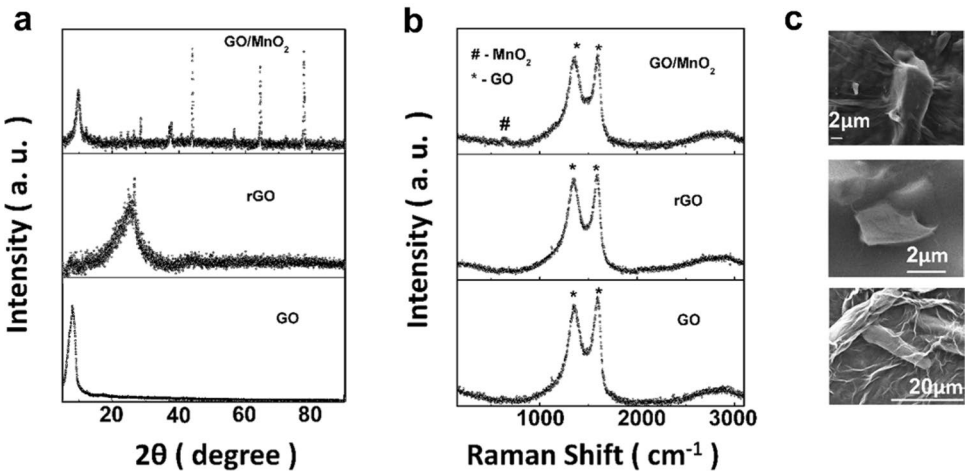

Fig. 3 **a** XRD plots, **b** Raman spectra and **c** SEM images of GO, rGO, and GMC-free-standing films

150–3100 cm^{-1} at room temperature. The bottom panel of Fig. 3b represents Raman spectrum of GO showing the presence of bands at 1357, 1598, and 2835 cm^{-1} in accordance with D, G and 2D bands of graphitic carbon, respectively [46–48, 52]. The center panel in Fig. 3b shows the Raman spectrum of rGO free-standing film, while the topmost panel in Fig. 3b represents the Raman spectrum of the GMC free-standing film in which presence of MnO_2 can be observed as a weak peak at 634 cm^{-1} [54]. The SEM images in Fig. 3c shows the presence of wrinkles and folds in the GO film (bottom panel), which are largely absent in rGO film (middle panel of Fig. 3c). The SEM image of the GMC film shows uniformly distributed MnO_2 particles intercalated into GO (top panel).

3.2 Humidity sensing data

Introduction of humid ambient air led to decrease in the resistance (R_h) of the film in comparison to that of the film measured in a non-humid mixture of N_2/O_2 (R_0), while it increased upon flushing out the humid air. On the other hand, degassing of the chamber led to retain its original resistance value. We have avoided heating the sensor for degassing purpose and instead preferred vacuum degassing so that all the functional groups on GO surfaces can be retained.

Figure 4a shows the resistive behavior of the free-standing films of GO, rGO, and GMC when exposed to different humidity percentages in the range from 26 to 90%. It is observed that at 26% of humidity, the resistance of the GO film changes from 120 to 80.9 MΩ, while that of rGO and GMC films change to 80.1 and 88.9 MΩ, respectively. It is to be noted that the multimeter used in our experiment is limited in its upper range by 120 MΩ and hence any values above 120 MΩ are also reported as 120 MΩ. Figure 4b shows that the recovery time of 7 s and response time of 16.7 s for GO film when exposed to 26% humidity. Response and recovery times are calculated by the amount of elapsed time between two dotted lines designated as start and end (Fig. 4b). Figure 4d, f show the response and recovery times of 2.3 and 0.6 s for rGO film and 1.9 and 0.8 s for GMC film, respectively at 26% humidity. It is also observed that at low exposure to humidity (26%), the change in the resistance is rather small in all the three films which increase rapidly when exposed to higher (> 26%) humidity levels.

Figure 5 summarizes the response of the free-standing films at 26 and 90% humidity, respectively. It can be observed that rGO free-standing film shows a higher response and recovery when compared to other free-standing films. Moreover, sensitivity to humidity is also higher for rGO film when compared to that of other films at higher humidity (90%). It can be concluded by comparing the change in resistance between all the three films that rGO is not only more sensitive to humidity but also is the fastest. Incorporation of MnO_2 causes lowering of the response as compared to that of GO but with faster response time.

Figure 6 plots the dynamic sensing responses of the free-standing films as a function of increasing humidity. It is evident that the GO film shows (Fig. 6a) a typical exponential behavior in its response to humidity whereas the other two films show a very slow increase in increased humidity. Figure 6b shows the bar chart of the response of all three films as a function of increasing humidity.

Robustness of the GO sensor was checked by exposing 90% humidity and observing the change in resistance. It was observed that the initial resistance of the GO film could be recovered by flushing out the humidity and thus indicates high operational stability (see Fig. 7).

3.3 Current (I)–Voltage (V) Characteristic of the free-standing film

Current–voltage (I–V) response of the free-standing films was observed before exploring its sensing response. The measurement was performed in vacuum (10^{-3} torr) using

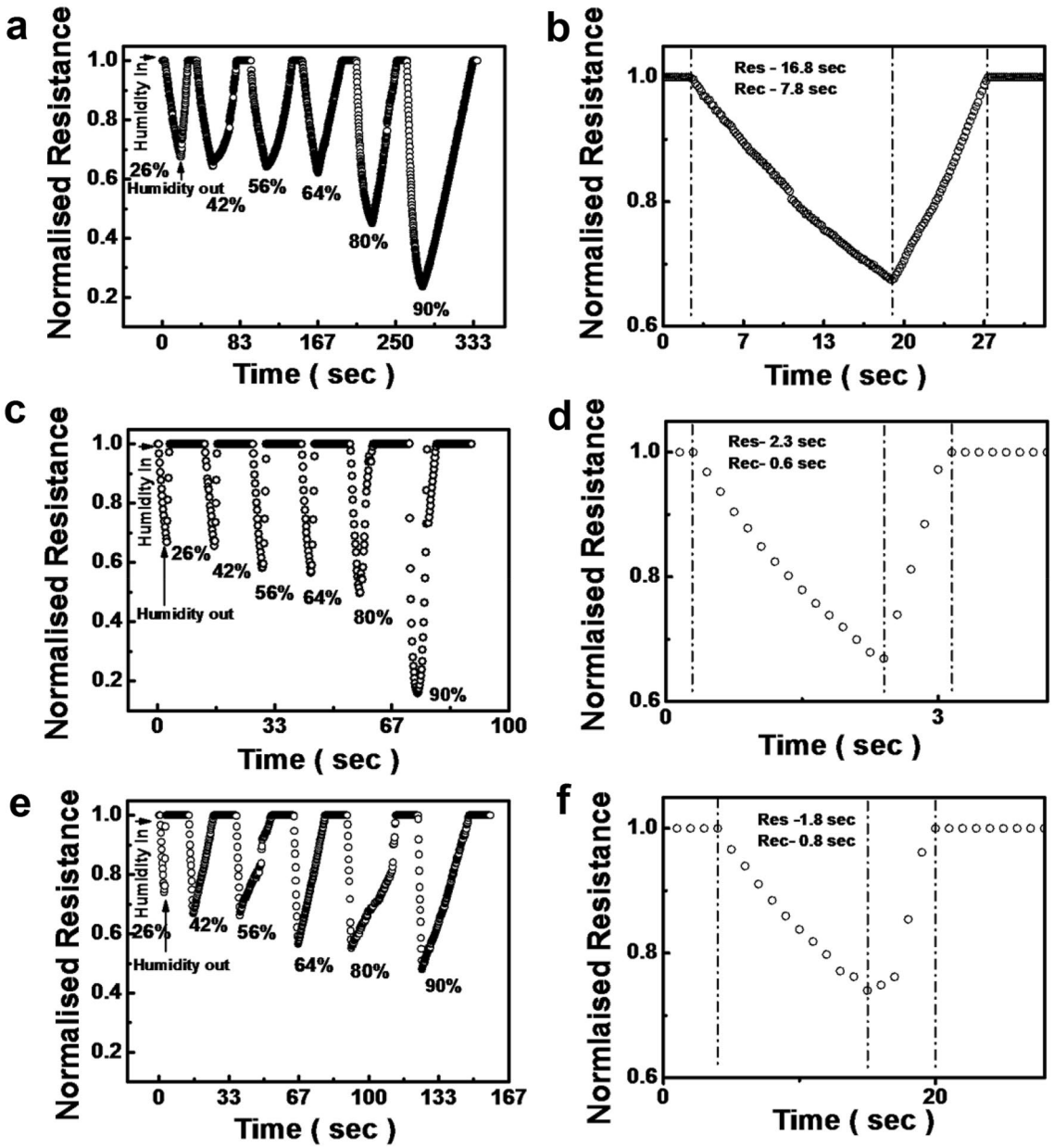

Fig. 4 Dynamic resistance-time response recorded at room temperature from **a** GO, **c** rGO and **e** GMC films; **b, d** and **f** are expanded plots of the resistance-time response at room temperature and 26% humidity GO, rGO and GMC, respectively

a Keithley 2420 source meter. From Fig. 8 it is observed that GMC film has the highest resistance in comparison to GO and rGO film, while rGO film has the lowest resistance concerning to GO and GMC film.

3.4 Sensing mechanism

3.4.1 Humidity sensing

The resistance of all the free-standing films decreased when exposed to humidity which indicates that electrons are transferred to the surface of the film by hydronium ions of water vapor thus making the film less resistive. When water vapor present in the gas (humid air) gets in contact with the negatively charged surface (functional groups) of GO, the formation of hydronium (H_3O^+) ion occurs at the surface [55–57]. Hydronium ion works as a charge carrier for proton-exchange between the GO films [56]. Humid air also gets adsorbed at the junctions (probe contacts) resulting in adsorption at the interfaces leading to an increase in the Ohm-contact resistance [56]. However, the increase in Ohmic-contact resistance is superseded by its decrease due

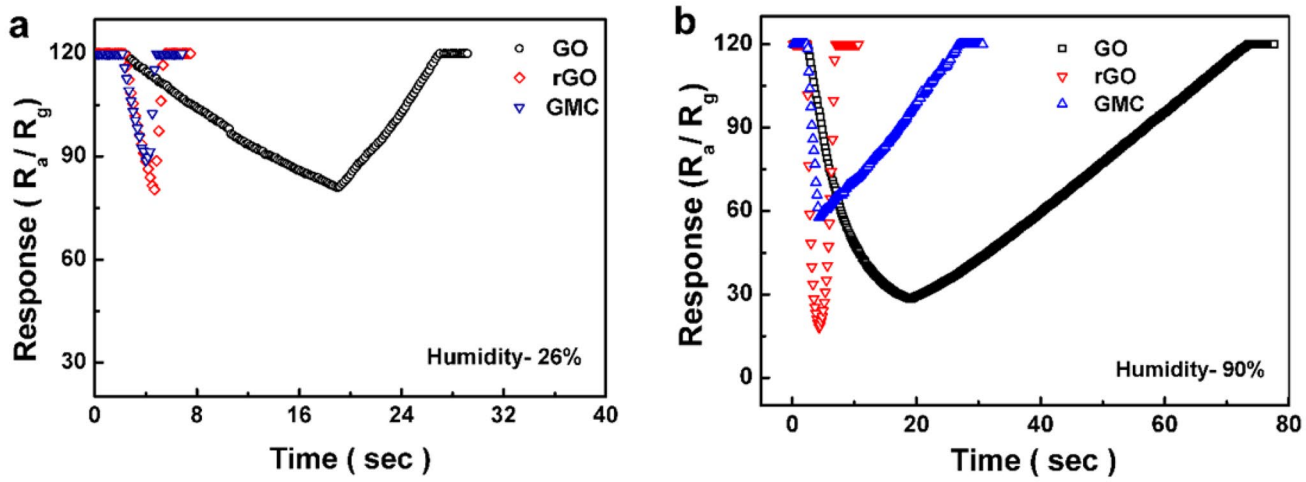

Fig. 5 Sensing responses of the free-standing films of GO, rGO, and GMC when exposed to **a** 26% and **b** 90% humidity respectively

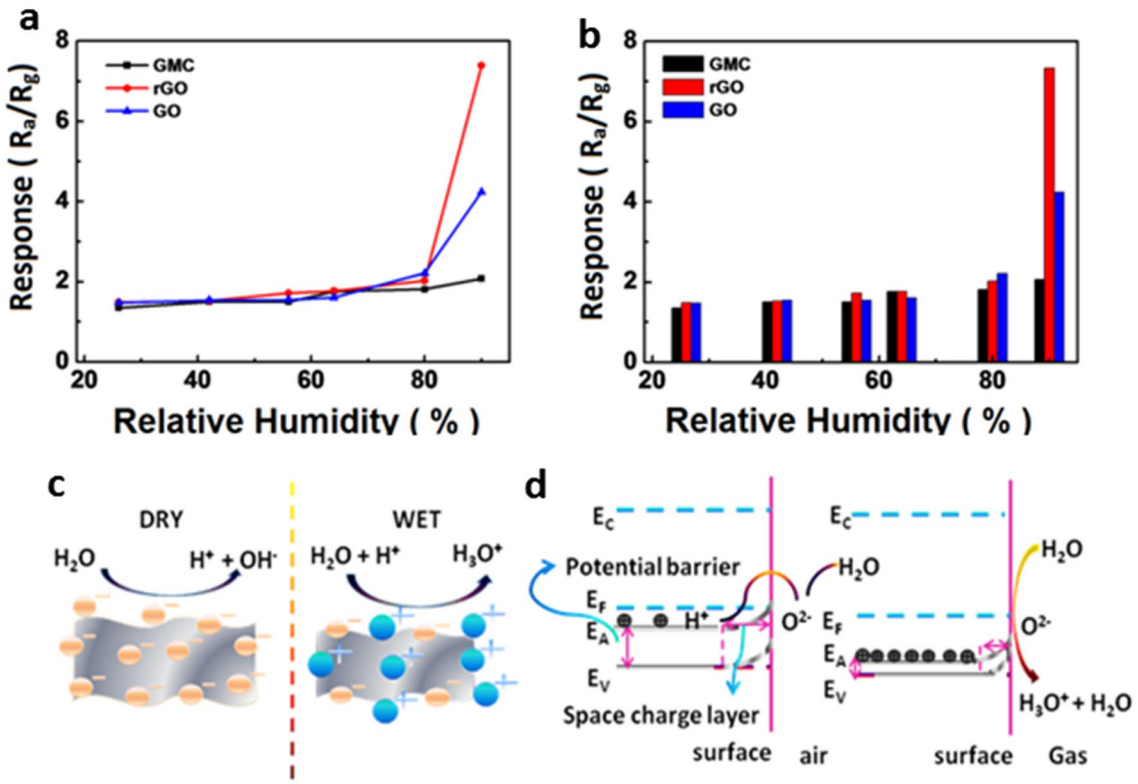

Fig. 6 **a** Dynamic response of free-standing films as a function of humidity, and **b** Bar chart comparison of the response of free-standing film, **c** Schematic of the process, and **d** band diagram of graphene oxide surface on adsorption of analyte

to adsorption phenomena and hence overall a decrease in the resistance of the free-standing film occurs [56].

GO layers consist of oxygen functional groups (OFGs) [58] due to which it has a high value of resistance, primarily due to the presence of ketonic groups. Thus, OFGs reduce surfaces conductivity of GO (see Fig. 6c) by binding the electrons at the surface and enabling an increase in the space charge layer (see Fig. 6d) [58, 59]. In case of GO free-standing film at higher humidity, the water molecules get intercalated into the stacked layer of GO and thus leads to an increase in resistance [36]. This increase in resistance results to an overall minimal change in resistance to GO film at higher humidity. This leads to the observance of a higher degree of change in the order of resistance of rGO film when

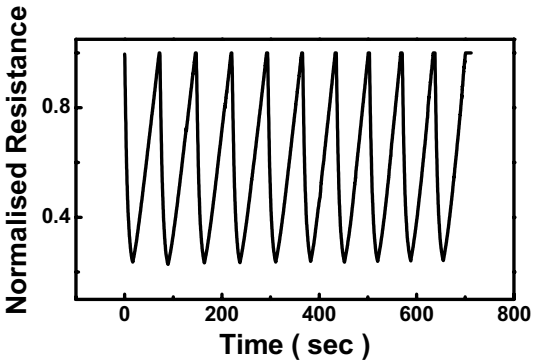

Fig. 7 Gassing–degassing cycles for free-standing GO films at 90% humidity

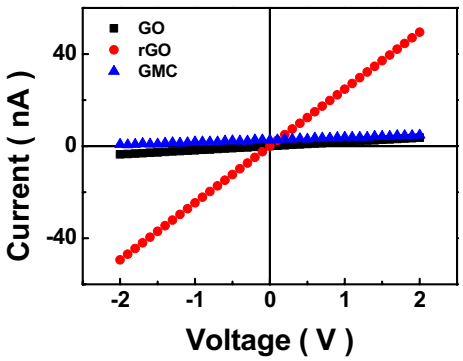

Fig. 8 I–V of GO, rGO and GMC film

compared to GO film at humidity up to 60%. Since rGO contains a lesser amount of functionalization compared to GO, the effect of hydrophobicity in rGO makes it a more effective at higher humidity content (> 60%) than GO film (hydrophilic). In the case of GMC film, incorporation of n-type metal oxide (MnO_2 particles) further increases the resistance due to the p–n junction effect [51, 52] at the surface boundary between p-type GO [48] and n-type metal oxide. MnO_2 behaves like n-type [60, 61] semiconductor due to the incorporation of oxygen at lattice sites, but overall GMC would have still p-type nature because the free holes in GO are far higher than electrons released by MnO_2. Oxygen from air binds at the surface of metal oxide and extracts the free electron at the surface of MnO_2 from the vacancy site, thus leading to a sudden decrease in the amount of free electron released back to the GO surface [58].

Moreover, adsorption of water molecule leads to increase in interlayer distance between the free-standing film and thus increases the distances between nanoparticles leading to change of ohmic contact to ohmic/capacitive contact [56]. This process is not entirely reversible, due to which GMC films are not stable at the repeated exposure of humidity. However in case of rGO film, due to less number of the functional group at the surfaces in contrast to GO and its hydrophobic behavior, on exposure to repeated humidity at the higher percentage change in resistance is almost comparable after 64% till 90% humidity. In case of GO film due to the presence of more number of functional groups in contrast to rGO film it shows stability at even 90% humidity.

3.4.2 Hydrogen peroxide sensing

Experimental results show that free-standing GO can be very promising material for hydrogen peroxide sensing at room temperature. In order to understand the mechanism of H_2O_2 sensing by GO, we note that p-type GO [48] has a hole depletion region near the interface due to which the electrical conductivity of the film is much less than n-type rGO. The decomposition of H_2O_2 on metal surface occurs through the following equations [62].

$$Mn^{+n}_{(surf)} + H_2O_2 = Mn^{+n+1}_{(surf)} + OH_{(aq)} + HO^{\circ}_{(aq)} \quad (3)$$

$$HO^{\circ}_{(aq)} + H_2O_{2(aq)} = HO^{\circ}_{2(aq)} + H_2O_{(aq)} \quad (4)$$

$$HO^{\circ}_{2(aq)} + Mn^{+n+1}_{(surf)} = Mn^{+n}_{(surf)} + H^{+}_{(aq)} + O_2 \quad (5)$$

$$H_2O + HO_2^{-} \rightarrow H_3O^{+} + O_2 \quad (6)$$

Interaction of hydrogen peroxide with metal ions produces hydroxyl and hydroperoxyl (HO_2). The hydroperoxyl further takes part in reaction with water molecules and gives hydrogen ion to water molecules to form hydronium ion [63, 64]. This formation of hydronium ion further follows the same mechanism (see Fig. 6c, d) as discussed for humidity sensing, thus leading to a decrease in resistance of the film.

The sensitivity of GO, rGO and GMC film in case of hydrogen peroxide sensing is calculated by using Eq. (7).

$$\text{Response } (\Delta R/R) = \left(R_{H_2O_2} - R_0\right)/R_0 \quad (7)$$

where, $R_{H_2O_2}$ and R_0 are the resistances of the film before and after the exposure of hydrogen peroxide gases respectively at a concentration of 83.5, 66.8, 50, 33.4 and 16.7 ppm. Figure 9a, c, e corresponds to sensing the response of GO, rGO and GMC free-standing film at different ppm of hydrogen peroxide analyte. While Fig. 9b, d, f represents response and recovery time of film at 16.5 ppm.

It is observed from Fig. 9a, c, e that upon addition of metal oxide to GO (GMC film), change in resistance is maximum (16.5 ppm) when compared to GO and rGO film. We have measured changes of 23.2, 31.7 and 33.5% in the resistance of the GO, rGO and GMC film, respectively. This led us to conclude that addition of metal oxide like MnO_2 (GMC

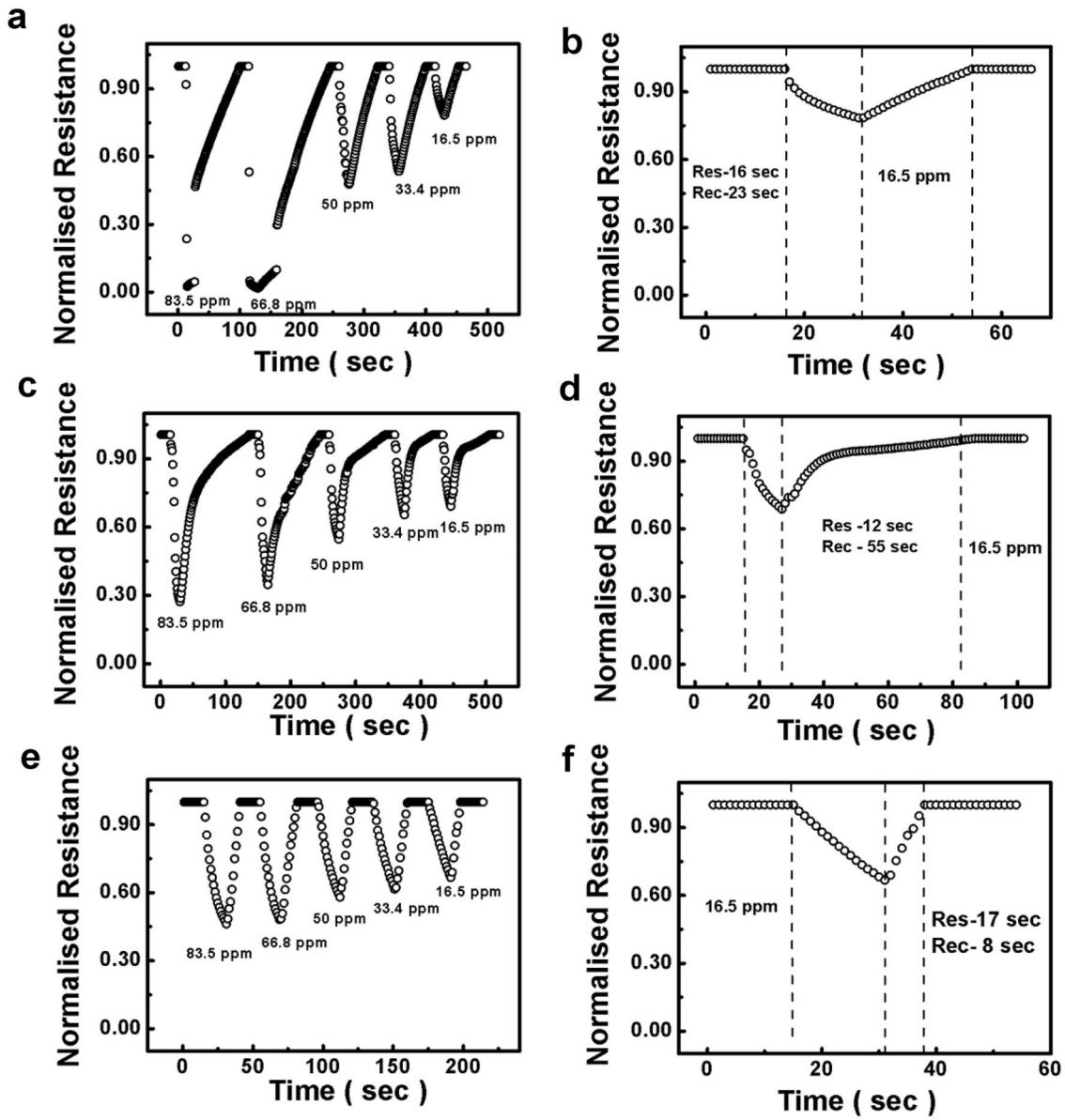

Fig. 9 Dynamic resistance-time response recorded at room temperature from **a** GO, **c** rGO and **e** GMC films; **b, d** and **f** are expanded plots of the resistance-time response at room temperature and 16.5 ppm for GO, rGO,and GMC, respectively

film) makes GO film more sensitive than any other film at a lower concentration of H_2O_2. This was also supported by the dynamic response plot of the free-standing film. It can be seen from Fig. 10 ($\Delta R = R_a - R_g$) that at a lower concentration of hydrogen peroxide GMC film is more sensitive followed by rGO and GO film.

4 Conclusion

Free-standing GO, rGO and GMC films have been developed for application as humidity and hydrogen peroxide sensors. Phase purity and morphology of the as-prepared free-standing films have been investigated by XRD, Raman spectroscopy, and SEM respectively. TGA of the GO, rGO and GMC films reveals higher thermal stability of GMC film. Resistance measurements on the free-standing films showed that the rGO free-standing film is more sensitive to humidity compared to GO and GMC free-standing films, as a change in resistance in rGO film is more than GO and GMC film. Intercalation of humidity between layers to GO is found to be the prominent reason behind less change in resistance at higher humidity as compared to rGO film. The fabricated GO free-standing film sensor also showed great stability at 90% humidity. Tuning of the response and recovery time due to the addition of MnO_2 in GO film is

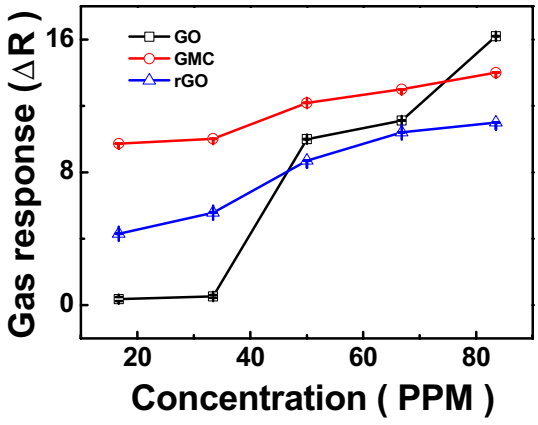

Fig. 10 Dynamic response of free-standing films as a function of H_2O_2 concentration

demonstrated. Role of metal oxide (MnO_2) in the detection of hydrogen peroxide has been investigated, and its sensing mechanism has been elaborated.

References

1. D. Zhang, N. Yin, C. Jiang, B. Xia, J. Mater. Sci. Mater. Electron. **28**, 2763 (2017)
2. G. Hassan, J. Bae, C.H. Lee, A. Hassan, J. Mater. Sci. Mater. Electron. **29**, 5806 (2018)
3. S. Sakai, T. Satow, K. Imakawa, K. Nagaoka, Anim. Sci. J. **81**, 694 (2010)
4. T. Yamamoto, Hyomen Kagaku **5**, 255 (1984)
5. Y. Yao, X. Chen, H. Guo, Z. Wu, X. Li, Sens. Actuators B **161**, 1053 (2012)
6. M.L. Yola, T. Eren, N. Atar, Sens. Actuators B **210**, 149 (2015)
7. H. Peroxide, G. Information, ATSDR **22**, 1 (2004)
8. E.A. Veal, A.M. Day, B.A. Morgan, Mol. Cell **26**, 1 (2007)
9. J. Hong, Z. Dai, Sens. Actuators B **140**, 222 (2009)
10. C. Zhao, H. Zhang, J. Zheng, J. Mater. Sci. Mater. Electron. **28**, 14369 (2017)
11. N. Kannadasan, N. Shanmugam, K. Sathishkumar, S. Cholan, R. Poonguzhali, G. Viruthagiri, J. Mater. Sci. Mater. Electron. **25**, 5137 (2014)
12. A. Din, S.B. Khan, M.I. Khan, S.A. Bin Asif, M.A. Khan, S. Gul, K. Akhtar, A.M. Asiri, J. Mater. Sci. Mater. Electron. **28**, 1092 (2017)
13. H. Bader, V. Sturzenegger, J. Hoigné, Water Res. **22**, 1109 (1988)
14. A.F. Lagalante, P.W. Greenbacker, Anal. Chim. Acta **590**, 151 (2007)
15. C. Matsubara, N. Kawamoto, K. Takamura, Analyst **117**, 1781 (1992)
16. G. Eranna, B.C. Joshi, D.P. Runthala, R.P. Gupta, Crit. Rev. Solid State Mater. Sci. **29**, 111 (2004)
17. C.-Y. Lee, G.-B. Lee, Sens. Lett. **3**, 1 (2005)
18. D. Zhang, J. Liu, H. Chang, A. Liu, B. Xia, RSC Adv. **5**, 18666 (2015)
19. T. Rahmani, H. Bagheri, M. Behbahani, A. Hajian, A. Afkhami, Food Anal. Methods (2018). https://doi.org/10.1007/s12161-018-1280-4
20. P. Hashemi, H. Bagheri, A. Afkhami, Y.H. Ardakani, T. Madrakian, Anal. Chim. Acta **996**, 10 (2017)
21. H. Bagheri, E. Ranjbari, M. Amiri-Aref, A. Hajian, Y.H. Ardakani, S. Amidi, Biosens. Bioelectron. **85**, 814 (2016)
22. H. Bagheri, A. Afkhami, H. Khoshsafar, M. Rezaei, S.J. Sabounchei, M. Sarlakifar, Anal. Chim. Acta **870**, 56 (2015)
23. H. Bagheri, A. Afkhami, P. Hashemi, M. Ghanei, RSC Adv. **5**, 21659 (2015)
24. S. Chakraborty, A.K. Chakraborty, M. Barbezat, G.P. Terrasi, Polym. Compos. (2017). https://doi.org/10.1002/pc.24675
25. S.S. Varghese, S. Lonkar, K.K. Singh, S. Swaminathan, A. Abdala, Sens. Actuators B **218**, 160 (2015)
26. S. Prezioso, F. Perrozzi, L. Giancaterini, C. Cantalini, E. Treossi, V. Palermo, M. Nardone, S. Santucci, L. Ottaviano, J. Phys. Chem. C **117**, 10683 (2013)
27. M.L. Yola, V.K. Gupta, T. Eren, A.E. Şen, N. Atar, Electrochim. Acta **120**, 204 (2014)
28. M.L. Yola, V.K. Gupta, N. Atar, Mater. Sci. Eng. C **61**, 368 (2016)
29. M.L. Yola, T. Eren, N. Atar, H. Saral, I. Ermiş, Electroanalysis **28**, 570 (2016)
30. M.L. Yola, T. Eren, N. Atar, Electrochim. Acta **125**, 38 (2014)
31. M.L. Yola, N. Atar, Z. Üstündağ, A.O. Solak, J. Electroanal. Chem. **698**, 9 (2013)
32. M.L. Yola, N. Atar, T. Eren, H. Karimi-Maleh, S. Wang, RSC Adv. **5**, 72590 (2015)
33. ÖA. Yokuş, F. Kardaş, O. Akyildirim, T. Eren, N. Atar, M.L. Yola, Sens. Actuators B **233**, 47 (2016)
34. V.K. Gupta, M.L. Yola, M.S. Qureshi, A.O. Solak, N. Atar, Z. Üstündağ, Sens. Actuators B **188**, 1201 (2013)
35. V.K. Gupta, M.L. Yola, N. Atar, Z. Ustundagì, A.O. Solak, Electrochim. Acta **112**, 541 (2013)
36. S. Elçin, M.L. Yola, T. Eren, B. Girgin, N. Atar, Electroanalysis **28**, 611 (2016)
37. N. Atar, T. Eren, M.L. Yola, Thin Solid Films **590**, 156 (2015)
38. N. Atar, T. Eren, B. Demirdögen, M.L. Yola, M.O. Çağlayan, Ionics (Kiel). **21**, 2285 (2015)
39. H. Zeinali, H. Bagheri, Z. Monsef-Khoshhesab, H. Khoshsafar, A. Hajian, Mater. Sci. Eng. C **71**, 386 (2017)
40. S. Gupta Chatterjee, S. Chatterjee, A.K. Ray, A.K. Chakraborty, Sens. Actuators B **221**, 1170 (2015)
41. K. Toda, R. Furue, S. Hayami, Anal. Chim. Acta **878**, 43 (2015)
42. G. Naik, S. Krishnaswamy, Graphene **05**, 1 (2016)
43. S. Borini, R. White, D. Wei, M. Astley, S. Haque, E. Spigone, N. Harris, J. Kivioja, T. Ryhänen, ACS Nano **7**, 11166 (2013)
44. S. Chen, R. Yuan, Y. Chai, F. Hu, Microchim. Acta **180**, 15 (2013)
45. B.C. Brodie, Philos. Trans. R. Soc. London **149**, 249 (1859)
46. W.S. Hummers, R.E. Offeman, J. Am. Chem. Soc. **80**, 1339 (1958)
47. D.C.C. Marcano, D.V.V. Kosynkin, J.M.M. Berlin, A. Sinitskii, Z.Z.Z. Sun, A. Slesarev, L.B.B. Alemany, W. Lu, J.M.M. Tour, ACS Nano **4**, 4806 (2010)
48. P. Ranjan, A. Kumar, A.D. Thakur, Mater. Today **5**, 732 (2018)
49. Y. Zhang, S. Zhu, X. Hao, C. Liu, Z. Wen, Ceram. Int. **40**, 13381 (2014)
50. J. Hao, Y. Zhong, Y. Liao, D. Shu, Z. Kang, X. Zou, C. He, S. Guo, Electrochim. Acta **167**, 412 (2015)
51. G. Han, Y. Liu, L. Zhang, E. Kan, S. Zhang, J. Tang, W. Tang, Sci. Rep. **4**, 1 (2014)
52. K. Krishnamoorthy, M. Veerapandian, K. Yun, S.J. Kim, Carbon N. Y. **53**, 38 (2013)
53. G. Huang, W. Kang, Q. Geng, B. Xing, Q. Liu, J. Jia, C. Zhang, Nanomaterials **8**, 215 (2018)
54. T. Gao, H. Fjellvåg, P. Norby, Anal. Chim. Acta **648**, 235 (2009)
55. Y. Tai, T.K. Bera, G. Lubineau, Z. Yang, J. Mater. Chem. C **5**, 3848 (2017)
56. Y. Tai, G. Lubineau, Small **13**, 1 (2017)

57. D. Zhang, J. Liu, B. Xia, IEEE Electron Device Lett. **37**, 916 (2016)
58. K.C. Lam, B. Huang, S.-Q. Shi, J. Mater. Chem. A **5**, 11131 (2017)
59. D. Chen, H. Feng, J. Li, Chem. Rev. **112**, 6027 (2012)
60. M. Hedden, N. Francis, J.T. Haraldsen, T. Ahmed, C. Constantin, Nanoscale Res. Lett. **10**, 292 (2015)
61. X. Xia, J. Electrochem. Soc. **136**, 266 (1989)
62. Y.N. Lee, R.M. Lago, J. Luis, G. Fierro, J. González, Appl. Catal. A **215**, 245 (2001)
63. J.-H. Lee, A. Katoch, S.-W. Choi, J.-H. Kim, H.W. Kim, ACS Appl. Mater. Interfaces **7**(5), 3101 (2015)
64. S. Mao, S. Cui, G. Lu, K. Yu, Z. Wen, J. Chen, J. Mater. Chem. **22**, 11009 (2012)